Ultrahigh-frequency surface acoustic wave generation for acoustic charge transport in silicon

S. Büyükköse,[1] B. Vratzov,[2] J. van der Veen,[1] P. V. Santos,[3] and W. G. van der Wiel[1]
[1]*NanoElectronics Group, MESA + Institute for Nanotechnology, University of Twente, P.O. Box 217, 7500 AE Enschede, The Netherlands*
[2]*NT&D–Nanotechnology and Devices, Wirichsbongardstr. 24, 52062 Aachen, Germany*
[3]*Paul-Drude-Institut für Festkörperelektronik, Hausvogteiplatz 5-7, 10117 Berlin, Germany*

(Received 29 November 2012; accepted 20 December 2012; published online 9 January 2013)

We demonstrate piezo-electrical generation of ultrahigh-frequency surface acoustic waves on silicon substrates, using high-resolution UV-based nanoimprint lithography, hydrogen silsequioxane planarization, and metal lift-off. Interdigital transducers were fabricated on a ZnO layer sandwiched between two SiO_2 layers on top of a Si substrate. Excited modes up to 23.5 GHz were observed. Depth profile calculations of the piezoelectric field show this multilayer structure to be suitable for acoustic charge transport in silicon at extremely high frequencies with moderate carrier mobility requirements. © *2013 American Institute of Physics*. [http://dx.doi.org/10.1063/1.4774388]

Surface acoustic waves (SAWs) travelling in a piezoelectric material have a piezoelectric potential wave accompanying the SAW strain field. In particular, the capability of SAWs to modulate a semiconductor system both mechanically and electrically enables them to control light, charge carriers, and excitons. Examples exploiting the acousto-optic and acoustoelectric interaction between SAWs and a material system comprise acousto-optic modulation,[1] photon detection/generation,[2,3] single-charge pumping,[4] acoustic spin transport,[5] acoustic switching,[6] and quantum information technology.[7] For acoustoelectric devices, most studies have been done on piezoelectric semiconductors, such as GaAs-based systems where the energy band diagram is modulated by the SAW-induced piezoelectric and strain fields. In such systems, SAW excitation is generally accomplished by an interdigital transducer (IDT), which is composed of interlocking finger electrodes. The period of the finger electrodes equals the SAW wavelength (λ_{SAW}) and determines the SAW frequency (f_{SAW}) together with the surface acoustic velocity of the material (v_{SAW}): $f_{SAW} = v_{SAW}/\lambda_{SAW}$. For weakly piezoelectric semiconductors, enhancement of the electromechanical coupling is normally achieved by introducing a piezoelectric thin film underneath the IDTs with a higher electromechanical coupling constant than the substrate. To provide piezoelectric potential modulation of the band structure in case of non-piezoelectric materials, this piezoelectric thin film needs to cover the whole surface, or at least the acoustic path. ZnO is a well-known material to enhance the electromechanical coupling of weakly piezoelectric materials or to excite SAWs even in non-piezoelectric substrates (such as silicon) because of its relatively large coupling coefficient.[8] As additional advantage, the presence of a thin ZnO film on top of a high-velocity substrate allows the excitation of overtones of the fundamental SAW mode with higher velocity, and hence a higher frequency owing to the "slow on fast" configuration.[1] However, being a reactive material, unprotected ZnO is CMOS incompatible, making it difficult to realize ZnO-based acoustoelectric devices on silicon chips. Efficient acoustoelectric charge transport by means of a SAW-induced potential modulation in Si requires strong SAW fields due to the lower electron and hole mobilities as compared to GaAs. These fields can be delivered by very high frequency SAWs due to the concentration the acoustic power near the surface. In the case that efficient acoustoelectric charge transport in silicon is accomplished, acoustic transport devices similar to those developed in GaAs-based systems are likely to be integrated into silicon circuits.

In this study, we have fabricated very high-frequency IDT devices on a $SiO_2/ZnO/SiO_2/Si$ layered structure and investigated the excited SAW modes both experimentally and theoretically. IDTs were fabricated by UV-based nanoimprint lithography and lift-off processes[9] with a SAW operation frequency as high as 23.5 GHz, using a ZnO film grown on a thermally oxidized Si substrate, covered with a 20 nm thick SiO_2 capping layer. This frequency is even higher than our recently reported highest frequency on Si using a ZnO film.[9] The present study is intended to investigate the potential for acoustoelectric applications in silicon-based structures.

As a substrate, a highly resistive Si (>10 kΩ) wafer was used. A high-quality thermal oxide layer with a thickness of 105 nm was grown on Si in an oven at 900 °C. ZnO films with thicknesses of 40 nm and 80 nm were grown on top of the SiO_2 layer by rf magnetron sputtering at 350 °C using an Ar/O_2 gas mixture. The deposition conditions were optimized in order to get the films hexagonal with the *c*-axis oriented (along the growth direction). This orientation is required for large piezoelectric coupling, and was verified by x-ray diffraction (XRD) measurements, shown in Fig. 1. The subsequent 20 nm SiO_2 layer, which was deposited in the same sputtering system, protected the ZnO film from being attacked by the lift-off solvent during the subsequent fabrication steps. For IDT fabrication, the samples were first spin coated with an 80 nm thick wet developable layer of WiDE-C 80 (Brewer Science) and baked at 150 °C. A 10 nm thick adhesion promoter layer of TranSpin™ (Moleculer Imprint, Inc.) was spin coated on top of the WiDE-C material to provide better adhesion of the NIL resist.

UV-based NIL was performed on an Imprio 55 tool by using the S-FIL™ process and MonoMat™ from Moleculer

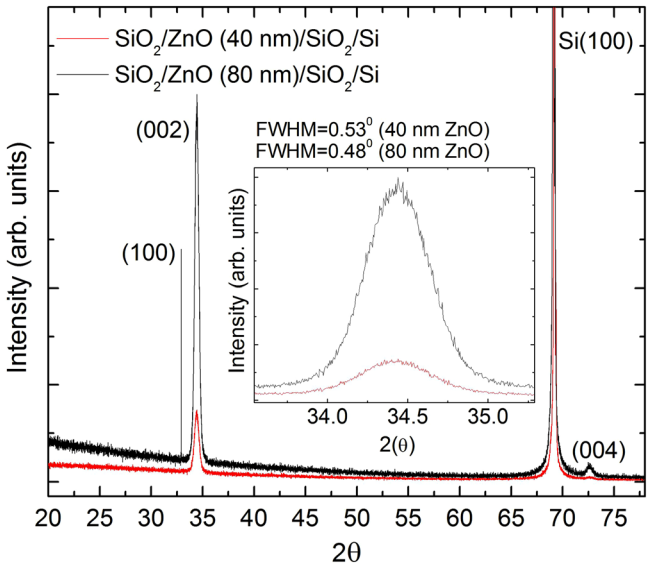

FIG. 1. XRD pattern and zoom in of the ZnO (002) peaks taken from SiO_2/ZnO/SiO_2/Si structures (inset). Results are showing the accurate *c*-axis orientation of the ZnO layers of 40 nm and 80 nm thickness with 0.53° and 0.48° of full width at half maximum (FWHM), corresponding to 16 nm and 17 nm grain sizes, respectively.

Imprints, Inc., as organic imprint resist. After nanoimprint, the samples were planarized with a 160 nm thick hydrogen silsequioxane (HSQ) layer by spin coating. For pattern transfer, reactive ion etching (RIE) was used. First, the HSQ layer was back-etched down to the top of the elevated imprint structures in a CHF_3-based plasma. Second, these elevated structures were etched down to the substrate in O_2-based RIE using the HSQ as an etch mask. The high etch resistance of HSQ functioned hereby as an etch mask providing an appropriate undercut profile for the final lift-off step. In the last step, 50 nm thick Al electrodes were deposited in an e-beam evaporation system followed by lift-off in 96% HNO_3. The process scheme and further details are described in our previous work.[9,10]

To study the SAW characteristics, two-port IDTs with single-finger (SF) and double-finger (DF) configurations were fabricated. The widths of the IDT finger electrodes were 125 nm, 100 nm, 80 nm, and 65 nm with metallization ratio 0.5, corresponding to acoustic wavelengths of four times and eight times the finger width for SF and DF IDTs, respectively. The IDT aperture was kept 30 μm for all devices and the input and output IDTs were separated by 306 μm and 405 μm for DF-IDTs and SF-IDTs, respectively.

In layered structures, the ratio between the SAW wavelength and the piezoelectric layer thickness determines the number of overtones. Emergence of overtones of the fundamental mode is more likely when the contrast in velocity between the overlayer and the substrate increases. In the present multilayer system, the SAW velocity of the Si substrate is larger than that of the ZnO film. The ZnO/SiO_2 films form, therefore, an acoustic waveguide, supporting overtones. The overtones are referred to as higher-order Rayleigh modes, with nodes in the depth direction. In contrast to a homogenous solid medium, SAW modes become dispersive in such a layered system.

Figure 2 shows the frequency response of two IDTs having acoustic wavelengths $\lambda_{SAW} = 1$ μm and 640 nm. The reso-

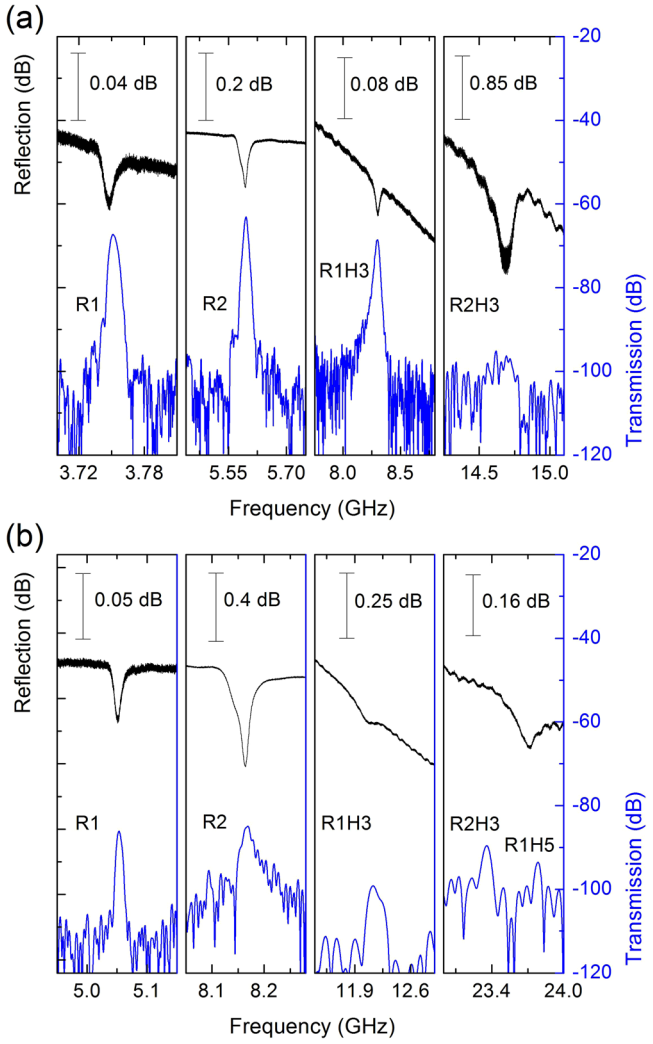

FIG. 2. Reflection (S_{11}) and transmission (S_{21}) spectra of DF-IDT devices with (a) 1 μm and (b) 640 nm wavelength. R1, R2, and R3 correspond to the first, second, and third order Rayleigh modes, respectively. H3 and H5 indicate the third and fifth harmonics. Reflection curves are vertically offset for clarity.

nance labeled R1 is associated with the first-order Rayleigh mode, which is the fundamental surface mode in piezoelectric materials. The other modes labeled R2 and R3 are associated with the second and third order Rayleigh modes, respectively. These modes have higher SAW velocities and thus resonances at higher frequencies. The peaks additionally labeled H3 and H5 show the third and fifth harmonics of related modes; for example, R2H3 indicates the third harmonic of the second mode. In order to correctly assign the SAW modes, the acoustic field distribution for each mode was obtained from numerical simulations based on a linear elastic model.[1]

Figure 3(a) compares the calculated and measured frequencies for all IDT devices. The calculations show very good agreement with the measured resonant frequencies. Figure 3(b) shows the calculated and measured acoustic velocities of the excited modes. In a layered system, the SAW velocity is expected to take a value between the bulk velocities of the low- and high-velocity material. For larger λ_{SAW}/d_{ZnO} ratio, the SAW velocity tends to increase. The acoustic field penetrates more into the higher-velocity Si

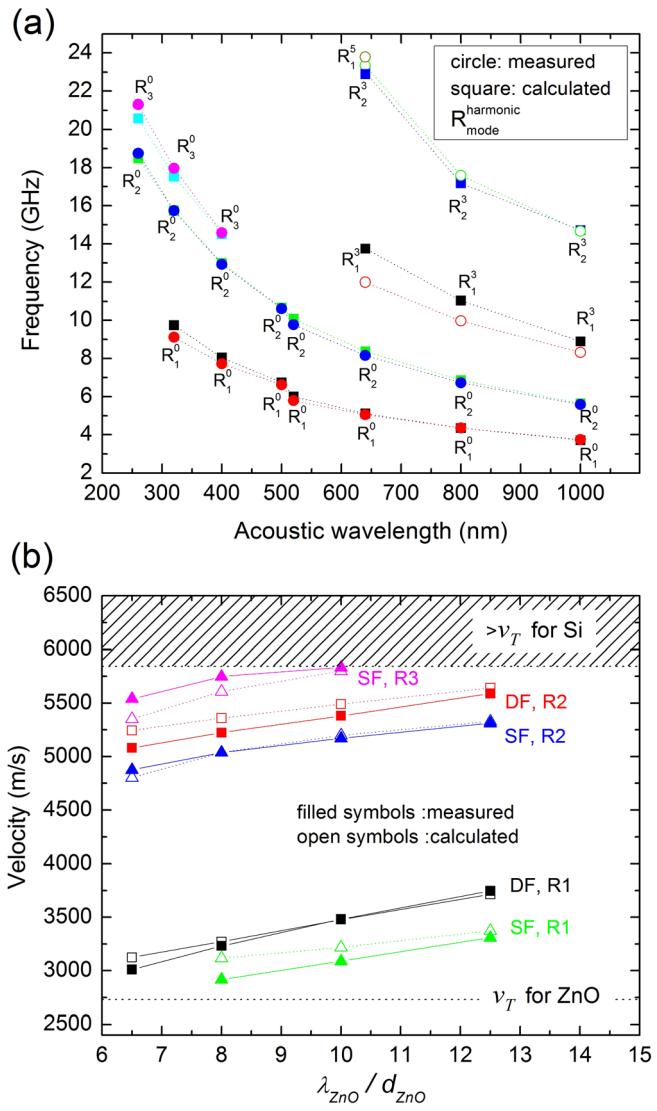

FIG. 3. Measured (circles) and calculated (squares) frequency (a) and velocity (b) of SAW modes. SF and DF refer to single- and double-finger IDTs, respectively. R1, R2, and R3 are first, second, and third order Rayleigh modes.

substrate, and the fraction of the acoustic field in Si increases, while that in the ZnO layer decreases, leading to a higher SAW velocity. The results show that the R1 and R2 SAW modes for DF-IDTs give a higher velocity than the same order modes for SF-IDTs at equal λ_{SAW}/d_{ZnO} ratios. This is the result of the thickness ratio of the ZnO and thermally grown SiO_2 layer (d_{ZnO}/d_{SiO2}), which is 0.38 and 0.76 for SF and DF-IDTs, respectively. The fraction of the acoustic field penetrating into the Si will be less for the SF-IDTs compared to the DF-IDTs for the same λ_{SAW}/d_{ZnO}, resulting in a lower acoustic velocity. The resonance frequency of the R3 mode for the SF IDT with 400 nm wavelength showed the highest measured velocity, 5833 m/s, which is very close to the predicted transverse bulk velocity of Si with polarization parallel to the *c*-axis ($v_T = (c_{44}/\rho)^{1/2} = 5845$ m/s). The two horizontal dashed lines indicate the transverse velocity (v_T) for Si and ZnO, respectively. A SAW mode with a velocity higher than v_T of the substrate is expected to couple with bulk modes and to show a leaky SAW nature, as the acoustic power flows into the bulk substrate resulting in very large insertion loss. Hence, 5845 m/s can be considered as an upper limit for non-leaky SAW modes in the present material system. As all of the measured velocities remain below this upper limit, the resonance modes measured in this study have non-leaky SAW nature.

For the acoustoelectric application of SAWs, the carrier drift velocity has great importance. The piezoelectric potential generated by a SAW modulates the energy band structure of the material within a depth of around one wavelength from the surface and creates mobile potential modulations moving along the acoustic path at sound velocity. These potential modulations can capture electrons (holes) in the minima (maxima) of the conduction (valence) band. Efficient transport requires the transport of carriers in the same wave cycle (or the same minima/maxima) along the transport path without loss. To satisfy this condition, the carriers should be able to follow the SAW-induced mobile potential modulations. Therefore, the minimum required mobility is $\mu_{min} = v_{SAW}/E_x$, where v_{SAW} is the SAW velocity and E_x is the piezoelectric field induced in the propagation direction. Electric field and potential distributions are determined by the acoustic linear power density P_l, which is defined as the total acoustic power flow per unit length across the acoustic beam (P_l = acoustic power/IDT aperture).

In order to prove that efficient acoustic charge transport (ACT) devices on SiO_2/ZnO/SiO_2/Si structure can be implemented at the high-frequency regime, calculations for the piezoelectric field (E_x) and potential distribution (Φ_{SAW}) were carried out with a nominal RF power $P_{RF} = 25$ dBm for different vibration modes. The power which is converted into the acoustic mode propagating in one direction was calculated from the amplitude of the dip in reflection (S_{11}) spectra. Calculations were carried out for both open (metal free) and short (metallized) surface conditions to reveal the effect of metal structures on the surface.

Figure 4 shows the depth dependence of E_x and Φ_{SAW} of the R1 and R2 modes, calculated for the IDT with 1 μm wavelength. A thin metal film deposited on the sputtered SiO_2 changes the surface condition and short circuits the

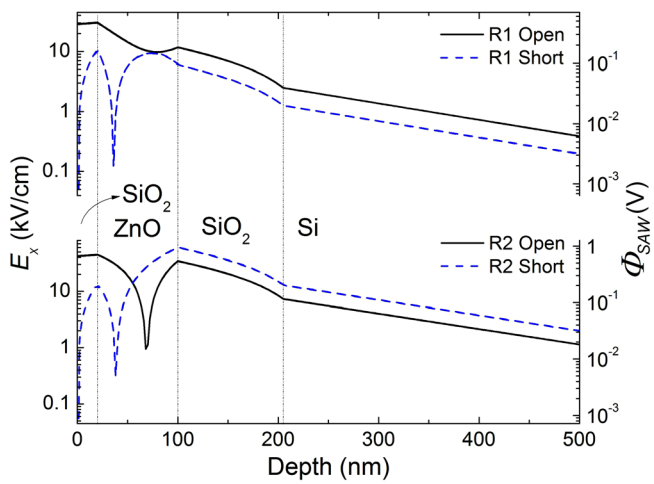

FIG. 4. Depth profile of piezoelectric field (E_x) and piezoelectric potential (Φ_{SAW}) for R1 and R2 modes in an IDT device with $\lambda_{SAW} = 1$ μm. The dashed and solid lines indicate a shorted (metallized) and open (non-metallized) surface condition.

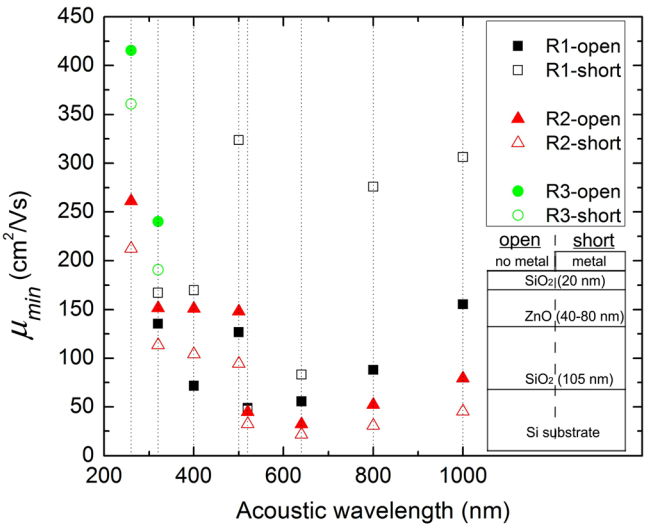

FIG. 5. The minimum required mobility μ_{min} for efficient acoustic charge transport at the SiO_2/Si interface for different SAW modes. The fundamental mode exhibits higher required mobility for the shorted surface condition. For higher-order modes, a metallized surface modifies the depth profile, giving a lower required mobility value. (Inset: The layer sequence and thicknesses).

piezoelectric potential, thus, changing the depth profile underneath. In the present material system, most of the acoustic transport in Si is expected at the SiO_2/Si interface located approx. 200 nm from the surface. For the R1 mode, the open surface condition gives a higher field value at the interface compared to the shorted surface. However, the R2 mode exhibits opposite characteristics for the short circuited surfaces. For the higher-order modes, the short circuited surface condition gives a much higher piezoelectric field value at the interface than that of the free surface condition. The minimum required mobility values calculated from E_x for the SiO_2/Si interface are given in Fig. 5. These values are less than both electron and hole mobilities at room temperature in intrinsic silicon.[11] In addition, the minimum mobilities in Fig. 5 are significantly lower than the reported value of 730 cm^2/V s by Barros *et al.*,[12] for a 750 MHz SAW with $P_l = 76$ W m^{-1} on ZnO/SiO_2/Si. In these experiments, this relatively high value was a limiting factor for ambipolar transport because of the low hole mobility.[12] The results of the Fig. 5 show that ultrahigh frequency SAWs can overcome this limitation problem for efficient hole transport.

In conclusion, we have fabricated ultrahigh frequency SAW devices up to 23.5 GHz on SiO_2/ZnO/SiO_2/Si by using a CMOS-compatible fabrication process. Excited modes were well verified by numerical calculations. Piezoelectric field distribution calculations showed that the SAW-induced field is strong enough for efficient charge (both electron and hole) transport at the Si/SiO_2 interface. Our results show that the higher-order modes are advantageous for charge transport since the increase the piezoelectric field. Additionally, metal structures on the SiO_2 surface modulating the piezoelectric field might be used as an acoustic charge guide for certain vibration modes to enhance the transport.

This research was supported by The Netherlands Technology Foundation (STW) within the NanoArrays project.

[1]M. M. de Lima, Jr. and P. V. Santos, Rep. Prog. Phys. **68**, 1639 (2005).
[2]V. I. Talyanskii, J. A. H. Stotz, and P. V. Santos, Semicond. Sci. Technol. **22**, 209 (2007).
[3]P. D. Batista, R. Hey, and P. V. Santos, Appl. Phys. Lett. **92**, 262108 (2008).
[4]V. I. Talyanskii, D. S. Novikov, B. D. Simons, and L. S. Levitov, Phys. Rev. Lett. **87**, 276802 (2001).
[5]T. Sogawa, P. V. Santos, S. K. Zhang, S. Eshlaghi, A. D. Wieck, and K. H. Ploog, Phys. Rev. Lett. **87**, 276601 (2001).
[6]V. I. Talyanskii, M. R. Graham, and H. E. Beere, Appl. Phys. Lett. **88**, 083501 (2006).
[7]S. Hermelin, S. Takada, M. Yamamoto, S. Tarucha, A. D. Wieck, L. Saminadayar, C. Bäuerle, and T. Meunier, Nature **477**, 435–438 (2011).
[8]E. A. Cerda-Méndez, D. Krizhanovskii, K. Biermann, R. Hey, P. V. Santos, and M. S. Skolnick, Superlattices Microstruct. **49**, 233 (2011).
[9]S. Büyükköse, B. Vratzov, D. Ataç, J. van der Veen, P. V. Santos, and W. G. van der Wiel, Nanotechnology **23**, 315303 (2012).
[10]S. Büyükköse, B. Vratzov, and W. G. van der Wiel, J. Vac. Sci. Technol. B **29**, 021602 (2011).
[11]*Landolt-Börnstein Tables*, edited by O. Madelung (Springer Verlag, Heidelberg, 1982), Vol. 17a.
[12]A. D. Barros, P. D. Batista, A. Tahraoui, J. A. Diniz, and P. V. Santos, J. Appl. Phys. **112**, 013714 (2012).